

## Dual Domain Filters based Texture and Structure Preserving Image Non-blind Deconvolution

Hang Yang, Ming Zhu  
Changchun Institute of Optics,  
Fine Mechanics and Physics  
Chinese Academy of Science  
China, Changchun 130033  
yanghang09@mails.jlu.edu.cn  
zhumingca@163.com

Yan Niu, Yujing Guan, Zhongbo Zhang  
Jilin University  
China, Changchun 130012  
{niuyan, guanyj, zhongbozhang}@jlu.edu.cn

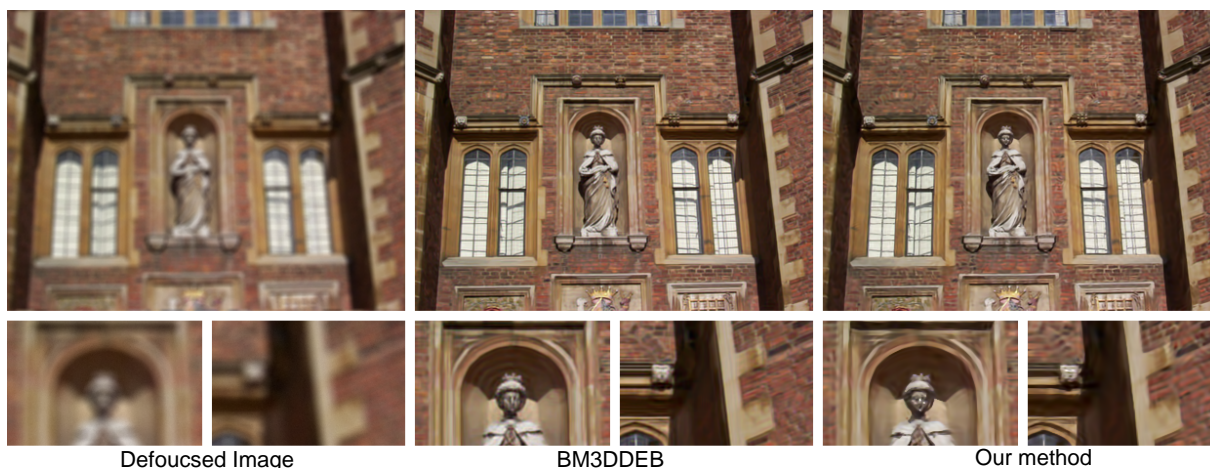


Figure 1. Removal of defocus blur in a photograph.

### Abstract

Image deconvolution continues to be an active research topic of recovering a sharp image, given a blurry one generated by a convolution. One of the most challenging problems in image deconvolution is how to preserve the fine scale texture structures while removing blur and noise. Various methods have been proposed in both spatial and transform domains, such as gradient based methods, nonlocal self-similarity methods, and sparsity based methods. However, each domain has its advantages and shortcomings, which can be complemented by each other. In this work we propose a new approach for efficient image deconvolution based on dual domain filters. In the deblurring process, we offer a hybrid method that a novel rolling guidance filter is used to ensure proper texture/structure separation, and then in the transform domain, we use the

short-time Fourier transform to recover the textures while removing noise with energy shrinkage. Our hybrid algorithm that is surprisingly easy to implement, and experimental results clearly show that the proposed algorithm outperforms many state-of-the-art deconvolution algorithms in terms of both quantitative measure and visual perception quality.

### 1. Introduction

Image deconvolution is a long-standing challenge in the field of computer vision and computational photography[1]. For example, the camera might have moved when capturing an image, resulting in an image corrupted by motion blur. Another common source of blurriness is out-of-focus blur.

The process of deconvolution is known to be an ill-posed

problem, even though the point spread function (PSF) is known, restoring coherent high frequency image details can still be very difficult.

In a typical deconvolution framework, a blurry image  $y$  is often modeled as a convolution between a PSF  $h$  and a sharp image  $u_{orig}$ , with additive noise  $\gamma$ :

$$y = \mathcal{H}u_{orig} + \gamma = h * u_{orig} + \gamma \quad (1)$$

In non-blind deconvolution, both  $y$  and  $h$  are given, and  $\gamma$  is often assumed to be i.i.d Gaussian with known variance  $\sigma^2$ . The deconvolution problem is to reconstruct  $u_{orig}$  from the observation  $y$ .

Image deconvolution methods can be broadly divided into two classes. The first class of methods relies on a pre-processing step followed by denoising, whereas the second class of methods is based on a variational optimization problem where the desired solution minimizes a criterion composed of fidelity and penalty terms.

The first category of methods apply a regularized inversion of the blur, followed by a denoising procedure. First, a regularized inversion of the blur is performed, such as Fourier regularization. This makes the image sharper, but also has the effect of amplifying the noise, as well as creating correlations in the noise. Then, a cleverly engineered denoising algorithm is used to remove artifacts and colored noise (non-flat power spectrum of the noise, not to be confused with color noise of RGB images). Various denoising methods have been used for this task: for instance, wavelet transform [2], a Gaussian scale mixture model (GSM) [3], a shape adaptive discrete cosine transform (SA-DCT)[4], or a block matching with 3D-filtering kernel regression (BM3D) [5].

The TV model[6],  $L_0$ -ABS[7], SURE-LET[8], Jia *et al*[9] and Yuan *et al* [10][11] belong to the second category. The TV model assumes that the  $l_1$ -norm of the gradient of the original image is small. It is well-suited for piecewise smooth images, and remarkably effective at preserving edges. Variations of this method have also been proposed in [12, 13, 14].  $L_0$ -ABS[7] is a sparsity-based deblurring method exploiting a fixed sparse domain. SURE-LET[8] method uses the minimization of a regularized *Steins* unbiased risk estimate (SURE) for designing deconvolution algorithms expressed as a linear expansion of thresholds. Jia *et al*[9] adopt a local sparse representation in image deconvolution. In [11], Yuan *et al* proposed a progressive inter-scale and intra-scale non-blind image deconvolution approach (PIEIAS) that significantly reduces the ringing artifacts.

In recent works, the sparsity and the self-similarity of natural images are usually combined to achieve better performance [15, 16, 17]. In [15], sparsity and self-similarity are separately characterized by two regularization terms, which are incorporated together into the final cost func-

tional of image restoration solution to enhance the image quality. In [16], a nonlocally centralized sparse representation (NCSR) model is proposed, which centralizes the sparse coding coefficients of the observed image to those estimates to improve the performance of sparse representation based image restoration.

Lately, low-rank modeling based approaches have also achieved great success in image restoration. Similar patches are grouped such that the patches in each group share similar underlying structure and form a low-rank matrix approximately. Finally, the matrix completion is carried out on each patch group to restore the image [18, 19, 20].

In this paper, we propose a novel patch-less image deconvolution method that integrates a rolling guidance filter [21] and a short-time Fourier transform(STFT) technique into the same framework. The rolling guidance filter is a novel structure preserving smoothing operator that can remove different levels of details in any input natural images. We propose an efficient iterative algorithm that consists of two parts: deblurring and denoising. The deblurring step amplifies and colors the noise, and corrupts the image information. Hence, in the denoising step, we use the rolling guidance filter to obtain a high-contrast image, and the residual image (texture and noise) is denoised in the short-time Fourier transform domain using energy shrinkage. The rolling guidance method can automatically refine edges that can be preserved in order to preserve large-scale structures optimally, but can not preserve low-contrast detail like textures without introducing noise. STFT shrinkage on the other hand results in good detail preservation, but suffers from ringing artifacts near steep edges. We integrate these two methods to produce a new deconvolution approach which outperforms many current state-of-the-art schemes. Apart from operating in different domains, the rolling guidance filter and the STFT shrinkage are very alike; hence, we call our method dual-domain filters based image deconvolution.

The remainder of this paper is organized as follows. Section 2 gives a brief overview of rolling guidance filter. Section 3 shows how the rolling guidance filter and SIFT are used for regularizing the deconvolution problem. Section 4 demonstrates the effectiveness of our approach via simulation. Section 5 provides concluding remarks.

## 2. Rolling guidance filter

Structure-preserving filtering is an essential operation with a variety of applications in computational photography and image analysis. Such an operation decomposes an image into prominent structure and fine-scale detail, making it easier for subsequent image manipulation.

Many of the structure-preserving smoothing operators are based on local filtering[22, 23, 24]. While these non-linear filters are simple and intuitive to use, they are often

ill-equipped to extract structure from texture due to the lack of explicit measures to distinguish the two. On the other hand, there are optimization-based[25, 26, 27] solutions, some of which have been specifically designed to handle texture and thus outperform local filtering in terms of texture removal. However, they usually come with additional level of complexity and sophistication, which makes them harder to implement, accelerate, scale, or adapt.

Recently, a novel method called rolling guidance filter [21] is proposed for nonlinear image decomposition based on a simple modification to bilateral filter[23]. It is in essence a joint bilateral filter (JBF) [28] that effectively removes texture while preserving structure, which the standard bilateral filter often fails to do. Being a simple extension to the popular bilateral filter, this method enjoys the benefits that come with it, such as simplicity, speed, ease of implementation, scalability, and adapt ability.

The rolling guidance filter first applies a Gaussian filter with variance  $\sigma_s^2$  to the image. When the image structure scale is smaller than  $\sigma_s$ , it will be completely removed in the filtered image. Structures of image are suppressed differently according to their sizes. We denote the convolution process with the input image  $I$  and Gaussian filter  $g_{\sigma_s}$  of variance  $\sigma_s$  as

$$\begin{aligned} L_{\sigma_s} &= g_{\sigma_s} * I \\ &= \frac{\sum_{q \in \mathcal{N}(p)} k_{p,q} I(q)}{\sum_{q \in \mathcal{N}(p)} k_{p,q}} \end{aligned} \quad (2)$$

where the Gaussian kernel is  $k_{p,q} = e^{-\frac{(p-q)^2}{2\sigma_s^2}}$ , and  $\mathcal{N}(p)$  is a square neighborhood window centered around pixel  $p$  with window radius  $r$ .  $L_{\sigma_s}$  is a blurred image, one can see that edges of structures with scales below the smoothing scale are completely removed according to the Gaussian average mechanism, while large-scale structures are blurred instead of eliminated. When applying Gaussian filter, the average of the edges removes nearly all texture patterns. For the large-scale intensity variation, Gaussian filter only blurs it and the edge can still be found.

So, the rolling guidance filter is composed of two main steps, i.e., small structure removal and edge recovery. The iterative edge recovery step forms the major contribution in this method. In this process, a guidance image  $J^t$  is iteratively updated. Initially,  $J^1$  is set as  $L_{\sigma_s}$  in Eq.(2). The value of  $J^{t+1}$  in the  $t$ -th iteration is obtained in a joint bilateral filtering form given the input  $I$  and the value in previous iteration  $J^t$ :

$$J^{t+1}(p) = \frac{\sum_{q \in \mathcal{N}(p)} k_{p,q} I(q)}{\sum_{q \in \mathcal{N}(p)} k_{p,q}} \quad (3)$$

where the bilateral kernel is:

$$k_{p,q} = e^{-\frac{(p-q)^2}{2\sigma_s^2}} e^{-\frac{(J^t(p)-J^t(q))^2}{2\sigma_r^2}} \quad (4)$$

$\sigma_s$  and  $\sigma_r$  control the spatial and range weights respectively.

This expression can be understood as a filter that smoothes the input  $I$  guided by the structure of  $J^t$ . This process is different by nature from how previous methods employ joint bilateral filter. Since this process uses  $J^t$  to compute the affinity between pixels, it makes resulting structures similar to  $J^t$ . Put differently, it yields structure transform from  $J$  to  $I$ .

**Algorithm 1** depicts final scale-aware rolling guidance filter construction:

---

**Algorithm 1: Rolling guidance filter**

1. Initialization:  $J^1 = L_{\sigma_s}, n_{itr}, \sigma_s, \sigma_r$
  2. for  $t = 1 : n_{itr}$ 

$$J^{t+1} = JBF(I, J^t, \sigma_s, \sigma_r) \triangleright \text{Eq.(3)}$$
 end
  3. Output:  $J^{n_{itr}+1}$ .
- 

The rolling guidance filter can remove small-scale structures while preserving other content, parallel in terms of importance to previous edge-preserving filter. This framework is simple to implement, greatly extensible to accommodate various tools for rolling guidance, and it yields decent performance. In our work, we first integrate this filter into the deconvolution problem. This leads to a powerful algorithm that obtains high quality results.

In Figure 2, we show an example about rolling guidance filter on noisy *Barbara* image. One can observe that the rolling guidance filtering result is a structure-preserving image without introducing noise, and texture and noise are in the residual image. Because the noisy image can be written as  $y = \delta * u_{orig} + \gamma$ , we use our dual domain filters "deconvolute" to the noisy image and compare it with BM3D denoising method[29].

### 3. Dual Domain Deconvolution

In this work, we intend to recover the underlying image by iteratively deblurring and denoising via dual domain filters(DDFs). Our method relies on two steps: (1) a regularized inversion of the blur in Fourier domain and (2) a denoising step using rolling guidance filter and short-time Fourier transform. In this section, we describe these two steps in detail.

#### 3.1. Direct deconvolution

The goal of deconvolution is to make a blurry image sharper. This has the positive effect of localizing information, but it has the negative side-effect of introducing new artifacts.

In our approach, we minimize the following energy function to estimate the noise-free image  $u$ .

$$\min_u \| y - h * u \|^2 + \lambda \| u - \mathbf{DDF}\mathbf{s}(u) \|^2 \quad (5)$$

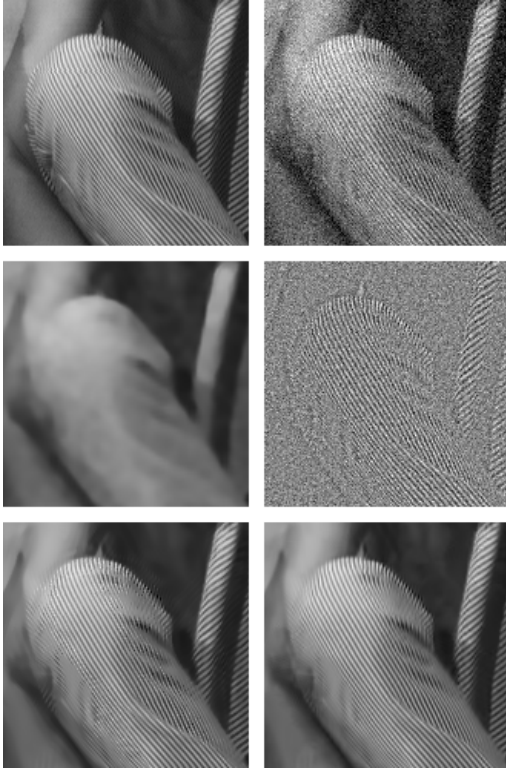


Figure 2. Visual quality comparison of image denoising on gray image *Barbara*. From left to right and top to bottom: original image, noisy image ( $\sigma = 20$ ), rolling guidance filtering result ( $\sigma_s = 7, \sigma_r = 0.05, n_{itr} = 2$ ), residual image, our denoised image (PSNR = 32.08dB), BM3D result [29] (PSNR=31.78dB).

Directly minimizing this energy is hard because  $\mathbf{DDFs}(\cdot)$  is highly nonlinear. We found that iterating the following two steps yields a good result in practice:

$$v^{k+1} = \arg \min_u \|y - h * u\|^2 \quad (6)$$

$$u^{k+1} = \mathbf{DDFs}(v^{k+1}) + \lambda^{k+1} \|u - u^k\|^2 \quad (7)$$

Considering that Eq.(6) is a simple least squares problem, we can update  $v$  with its analytic solution. In Fourier domain, this can be solved in a single step:

$$\mathcal{F}(v^{k+1}) = \frac{\mathcal{F}(h)^* \cdot \mathcal{F}(y) + \lambda^{k+1} \mathcal{F}(u^k)}{|\mathcal{F}(h)|^2 + \lambda^{k+1}} \quad (8)$$

by using the convolution theorem for Fourier transform, where  $\mathcal{F}$  is the FFT operator and  $\mathcal{F}(\cdot)^*$  denotes the complex conjugate. The plus, multiplication, and division are all component-wise operators.

For initialization, we set  $u^0$  to be zero (a black image). Solving Eq.(6) yields a noisy image  $v^k$  that also contains

useful high-frequency image structures. In the alternating minimization process, the noise in  $v^k$  is gradually reduced, while the high-frequency image details are preserved.

The regularization parameter  $\lambda^k$  strikes a balance between the data fidelity and regularity. In practice, we find that large  $\lambda^k$ s often cause noisy results with ringing effects, though they substantially reduce the noise variances. We should choose a smaller  $\lambda^k$  which obtains an edge preserving image with more noise. Then, in the denoising step, we propose a procedure that removes the leaked noise and additional image artifacts.

For an image of size  $N \times N$  at the  $k$ -th step, we compute the parameters  $\lambda^k$  by:

$$\lambda^0 = \frac{N^2 \sigma^2}{\|y - E(y)\|_2^2 - N^2 \sigma^2}$$

$$\lambda^{k+1} = \beta \lambda^k \quad (9)$$

where  $E(y)$  denotes the mean of  $y$ . From this equation, one can see that the larger variance of image ( $\|y - E(y)\|_2^2 - N^2 \sigma^2$ ) would obtain a smaller  $\lambda^0$ , it can be preserving the detail information, while the smaller variance of image (a smooth image) which contains a few high-frequency information will not produce the strong ringing effects with large  $\lambda^0$ .

Parameter  $\lambda$  is automatically adapted in iterations starting from a small value  $\lambda^0$ , it is multiplied by  $\beta$  each time. This scheme is effective to speed up convergence[12].

### 3.2. Dual domain denoising

To suppress the amplified noise and artifacts introduced by Eq.(6), we plan to apply the dual domain transform to denoise the estimated image  $v^k$  ( $\mathbf{DDFs}(v^k)$ ). We observe that spatial domain methods excel at denoising high-contrast images while transform domain methods excel at low-contrast images. We therefore separate the image into two layers, and denoise them separately. The rolling guidance filter is appropriate for this decomposition. The high-contrast layer is the rolling guidance filtered image, and the low-contrast layer (texture and noise) is the residual image. Since the high-contrast image is already denoised, it only remains to denoise the low-contrast image in the transform domain using shrinkage.

In the first step, we calculate the denoised high-contrast value using a rolling guidance filter. We use rolling guidance filter to filter the noisy image  $v^k$ , and obtain a filtered image  $v_r^k$ .

In the second step, we prepare for the energy shrinkage in the transform domain by extracting the low contrast images and performing the STFT. The STFT is a discrete Fourier transform (DFT) preceded by multiplication of the signal with a window function to avoid boundary artifacts. In this work, we choose the spatial Gaussian of the bilateral

kernel as the window function. The low contrast images can be obtained by subtracting the rolling guidance filtered value  $v_r^k$  from  $v^k$ . We define the coefficients  $VT_p^k$  and  $ST_p^k$  for frequencies  $m$  in the Fourier window  $\mathcal{M}_p$  with the same size as  $|\mathcal{N}(p)|$ .

$$VT_p^k(m) = \sum_{q \in \mathcal{N}(p)} (v_r^k(q) - v_r^k(p)) k_{p,q} e^{-\frac{i2\pi m \cdot (q-p)}{2r+1}} \quad (10)$$

$$ST_p^k(m) = \sum_{q \in \mathcal{N}(p)} (v^k(q) - v_r^k(p)) k_{p,q} e^{-\frac{i2\pi m \cdot (q-p)}{2r+1}} \quad (11)$$

In the last step, we shrink the noisy short-time Fourier coefficient  $ST_p^k$ . We use shrinkage factor similar to the range kernel of the Eq.(3). For the shrinkage factors  $Th_p^k$ , we want to keep the signal and discard the noise, so we take the reciprocal of the normalized Euclidean distance.

Under the assumption that the kernel  $k_{p,q}$  is noise-free, the variance  $\sigma_{k,p}^2$  of the noisy Fourier coefficients is

$$\sigma_{k,p}^2 = \sigma_k^2 \sum_{q \in \mathcal{N}(p)} k_{p,q}^2. \quad (12)$$

where  $\sigma_k^2$  is the variance estimated from  $v^k$ . The noise variance  $\sigma_k^2$  is an important parameter for dual domain filters, therefore we use the approach proposed in [30] to update the estimation of noise variance in the denoising step.

We define  $Th_p^k(m) = e^{-\frac{\eta \sigma_{k,p}^2}{|VT_p^k(m)|^2}}$ , where  $\eta$  plays a similar role as the bilateral range parameter  $\sigma_r$ . And the shrunk coefficients can be written as:

$$\widetilde{ST}_p^k(m) = Th_p^k(m) ST_p^k(m) \quad (13)$$

The inverse DFT over the frequency domain  $\widetilde{ST}_p^k$  is

$$\widetilde{st}_p^k(q) = \frac{1}{|\mathcal{M}(p)|} \sum_{m \in \mathcal{M}(p)} \widetilde{ST}_p^k(m) e^{\frac{i2\pi m \cdot (q-p)}{2r+1}} \quad (14)$$

As we are only interested in the value at the center pixel  $p$ , the low-contrast value is simply the mean of all shrunk coefficients, we denote this value by  $st^k(p)$ :

$$st^k(p) = \widetilde{st}_p^k(p) = \frac{1}{|\mathcal{M}(p)|} \sum_{m \in \mathcal{M}(p)} \widetilde{ST}_p^k(m) \quad (15)$$

Then, the original image can be approximated by the sum of the two denoised layers as:

$$\tilde{u}^k = v_r^k + st^k \quad (16)$$

The resulting image  $st^k$  usually contains a special form of distortions and introduces additional visual artifacts.

Since bilateral filter can effectively remove the edges of small magnitudes caused by these artifacts, we utilize it to suppress visual artifacts and leave the edges and texture of large magnitudes intact:

$$u^k = JBF(v^k, \tilde{u}^k, \sigma_s, \sigma_r) \quad (17)$$

We summarize the main steps of the proposed image deconvolution algorithm as shown in **Algorithm 2**

---

**Algorithm 2** : Image Deconvolution via Dual Domain Filters

---

1. Initialization:  $u^0 = 0$
  2. Iterate on  $k = 0, 1, \dots, iter - 1$ 
    - 2.1 Iterative regularization: obtain  $v^{k+1}$  using Eq.(8).
    - 2.2 Image denoising via dual domain filters:
      - 2.2.1 Rolling guidance filtering of  $v^{k+1}$  to obtain a high-contrast image  $v_r^{k+1}$ .
      - 2.2.2 Shrinkage the residual image  $v^{k+1} - v_r^{k+1}$  in the short-time Fourier domain to extract the low contrast image  $st^k$ .  $\triangleright$  Eq.(10)-Eq.(15)
      - 2.2.3 Sum of the two denoised layers:  $v_r^{k+1}$  and  $st^k$  to obtain  $\tilde{u}^{k+1}$ .  $\triangleright$  Eq.(16)
      - 2.2.4 Joint bilateral filtering of  $v^{k+1}$  using  $\tilde{u}^{k+1}$  as guidance image to obtain an improved denoised image  $u^{k+1}$ .  $\triangleright$  Eq.(17)
  3. Output :  $u^{iter}$ .
- 

## 4. Simulations

In this section, experiments are conducted to verify the performance of the proposed algorithm on image deconvolution.

In rolling guidance filter, we have found that the ISNR values generally reach the peak value when  $\sigma_s$  in [5,9]. We fixed this parameter value to 7 in our experiments. For the parameter  $\sigma_r$ , we found that a large value of it would result in a smooth image whereas a too small value would lead to inadequate denoising. The choice of this parameter is largely heuristic in nature. We have empirically found that  $\sigma_r$  in [0.03, 0.07] generally yields good results and have accordingly used  $\sigma_r = 0.05$  for the results in the experiments.

In STFT, for the shrinkage parameter  $\eta$ , we found that a large value of it would result in a textureless image whereas a too small value would lead to inadequate denoising. We have found that the ISNR values generally reach the peak value when shrinkage parameter in [0.25, 0.6]. We fixed this parameter value to 0.4 in our experiments. In theory, the Fourier coefficients  $ST_p^k$  in Eq.(11) are conjugate symmetric and  $Th_p^k$  is symmetric which makes  $\widetilde{ST}_p^k$  real. In practice, due to numerical errors,  $\widetilde{ST}_p^k$  may become complex, in which case we drop the imaginary part.

We set the iteration number  $n_{itr} = 2$  in the rolling guidance filter, and  $iter = 6$  in **Algorithm 2**. The choice of  $\beta$  Eq.(9) is taken as 1.5 which well balances efficiency and performance.

All the experiments are performed in Matlab 7.11.0 on a Pentium(R) Dual-Core CPU E5300 processor (2.60 GHz), 2.0G memory, and Windows Xp operating system. To give an estimate of the complexity of the proposed algorithm, we mention that, on a  $256 \times 256$  image, one iteration takes about 52 seconds, and about 6 iterations are typically sufficient.

The bottleneck is the transition from spatial to frequency domain. If this transition was a pure Gabor transform, we could exploit sliding window techniques to update the Fourier coefficients incrementally. However, since the signal is multiplied by an arbitrary range kernel, we need a per-pixel FFT with complexity  $O(N^2 \log N)$ . Thus, we implemented a  $C$  version using the FFTW library, which shortened the time to 31 seconds. Since the pixels are mutually independent, we achieved linear scalability using dual quad-core CPUs, reducing the time to 3.8 seconds.

In our set, six typical deblurring experiments (as shown in Table 1) with respect to four standard gray images, which have been presented in [7] and [5] are provided.

Scenario	PSF	$\sigma^2$
1	$1/(1 + i^2 + j^2)$ , for $i, j = -7, \dots, 7$	2
2	$1/(1 + i^2 + j^2)$ , for $i, j = -7, \dots, 7$	8
3	$9 \times 9$ uniform kernel (boxcar)	$\approx 0.3$
4	$[1 \ 4 \ 6 \ 4 \ 1]^T [1 \ 4 \ 6 \ 4 \ 1]/256$	49
5	$25 \times 25$ Gaussian with std = 1.6	4
6	$25 \times 25$ Gaussian with std = 0.4	64

Table 1. Experiment settings with different blur kernels and different values of noise variance  $\sigma^2$  for pixel values in  $[0,255]$ .

To evaluate the quality of there constructed image, the improvement in signal-to-noise-ratio (ISNR) is calculated to evaluate the visual quality. The ISNR is defined as

$$ISNR = 10 \log_{10} \left( \frac{\|u_{orig} - y\|_2^2}{\|u_{orig} - \hat{u}\|_2^2} \right), \quad (18)$$

where  $\hat{u}$  is the corresponding estimated image.

The proposed dual domain filters deconvolution method is compared with five recently developed deconvolution approaches, i.e., ForWaRD [2], FTVd [12], L0-ABS [7], SURE-LET [8], PIEIAS[11] and BM3DDEB [5]. We use the default parameters suggested by the authors for the competing algorithms.

The ISNR results on four gray test images in the set of experiments are reported in Table 2. From Table 2, we can see that the proposed algorithm achieves highly competitive performance compared with other leading deblurring



Figure 3. Visual quality comparison of image deblurring on gray image *Cameraman* ( $256 \times 256$ ). From left to right and top to bottom: original image, noisy and blurred image (scenario 4), the deblurred image by L0-ABS (ISNR=2.93dB), SURE-LET (ISNR=2.67dB), BM3DDEB (ISNR = 3.34dB), and our method (ISNR = 3.57dB).

methods. The highest ISNR results in the experiments are labeled in bold.

L0-ABS and SURE-LET produce slightly higher average ISNR than ForWaRD and FTVd, while our method outperforms L0-ABS by 1.2 dB for the scenario 3, outperforms PIEIAS by 0.79 dB for scenario 2, and outperforms SURE-LET by 2.6 dB for scenario 6, respectively. One can observe that BM3DDEB and our method produce very similar results, and obtain significant ISNR improvements over other competing methods. In average, proposed method outperforms BM3DDEB by (0.14dB, 0.40dB, 0.89dB, 0.25 dB, 0.23dB, and -0.083 dB) for the six settings, respectively. The visual comparisons of the deblurring methods are shown in Figures 3~6, from which one can observe that the our model produces cleaner and sharper image edges and textures than other competing methods.

In particular, for image *Barbara* ( $512 \times 512$ ) with rich textures, the proposed method outperforms current state-of-the-art methods BM3DDEB more than 1 dB in the scenario 2 with more textures and clearer edges than other competing methods, as shown in Figure 6.

Since the rolling guidance filter is highly nonlinear., it is difficult to give its theoretical proof for global convergence of proposed method. Here, we only provide empirical evidence to illustrate the stability of the proposed deconvolution method. Figure 7 plots the evolutions of ISNR versus iteration numbers for test images in the cases of scenario 3 (PSF =  $9 \times 9$  uniform kernel,  $BSNR = 40$ ) and scenario 4 (PSF =  $[1 \ 4 \ 6 \ 4 \ 1]^T [1 \ 4 \ 6 \ 4 \ 1]$ ,  $\sigma = 7$ ) for four test images. It is observed that with the growth of iteration

	Scenario						Scenario					
	1	2	3	4	5	6	1	2	3	4	5	6
Method	Cameraman (256 × 256)						House (256 × 256)					
BSNR	31.87	25.85	40.00	18.53	29.19	17.76	29.16	23.14	40.00	15.99	26.61	15.15
ForWaRD	6.76	5.08	7.40	2.40	3.14	3.92	7.35	6.03	9.56	3.19	3.85	5.52
FTVd	7.41	5.24	8.56	2.57	3.36	1.37	7.98	6.57	10.39	4.49	4.72	2.44
L0-Abs	7.70	5.55	9.10	2.93	3.49	1.77	8.40	7.12	11.06	4.55	4.80	2.15
SURE-LET	7.54	5.22	7.84	2.67	3.27	2.45	8.71	6.90	10.72	4.35	4.26	4.38
PIEIAS	8.10	6.14	9.23	3.41	3.49	4.65	8.94	7.76	11.22	4.85	4.94	7.07
BM3DDEB	8.19	<b>6.40</b>	8.34	3.34	3.73	<b>4.70</b>	9.32	8.14	10.85	5.13	4.56	<b>7.21</b>
Our Method	<b>8.26</b>	6.29	<b>9.42</b>	<b>3.57</b>	<b>3.78</b>	4.61	<b>9.48</b>	<b>8.30</b>	<b>12.17</b>	<b>5.32</b>	<b>5.20</b>	6.94

	Scenario						Scenario					
	1	2	3	4	5	6	1	2	3	4	5	6
Method	Lena (512 × 512)						Barbara (512 × 512)					
BSNR	29.89	23.87	40.00	16.47	27.18	15.52	30.81	24.79	40.00	17.35	28.07	16.59
ForWaRD	6.05	4.90	6.97	2.93	3.50	5.42	3.69	1.87	4.02	0.94	0.98	3.15
FTVd	6.36	4.98	7.87	3.52	3.61	2.79	3.10	1.33	3.49	0.63	0.75	0.59
L0-Abs	6.66	5.71	7.79	4.09	4.22	1.93	3.51	1.53	3.98	0.73	0.81	1.17
SURE-LET	7.71	5.88	7.96	4.42	4.25	4.37	4.35	2.24	6.02	1.13	1.06	1.20
PIEIAS	7.68	6.22	8.16	4.69	4.39	5.85	6.72	3.30	4.48	1.57	0.98	5.01
BM3DDEB	7.95	6.53	8.06	4.81	4.37	6.40	7.80	3.94	5.86	1.90	1.28	<b>5.80</b>
Our Method	<b>7.96</b>	<b>6.82</b>	<b>9.04</b>	<b>5.04</b>	<b>4.55</b>	<b>6.67</b>	<b>8.10</b>	<b>5.15</b>	<b>6.07</b>	<b>2.26</b>	<b>1.33</b>	5.56

Table 2. Comparison of the output ISNR(dB) of the proposed deblurring algorithm. BSNR(Blurred Signal-to-noise ratio) is defined as  $BSNR = 10 \log_{10} Var(y)/N^2\sigma^2$ , where  $Var(\cdot)$  is the variance.

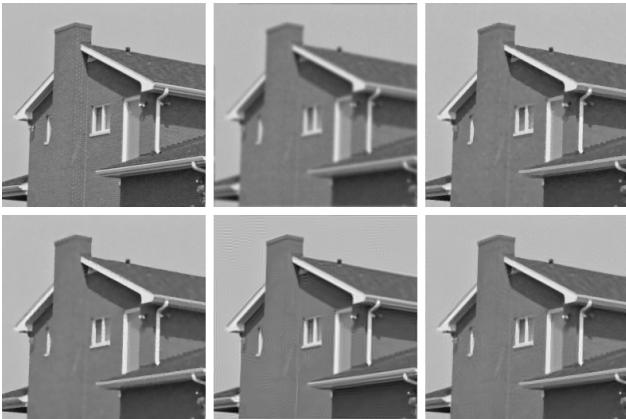


Figure 4. Visual quality comparison of image deblurring on gray image *House* (256×256). From left to right and top to bottom: original image, noisy and blurred image (scenario 5), the deblurred image by FTVd (ISNR=4.72dB), PIEIAS (ISNR=4.94dB), BM3DDEB (ISNR = 4.56dB ), and our method (ISNR = 5.20dB).



Figure 5. Details of the image deconvolution experiment on image *Lena* (512×512). From left to right and top to bottom: Crop from original image, noisy and blurred image (scenario 3), L0-Abs (ISNR=7.79dB), the deblurred image by PIEIAS (ISNR=8.16dB), BM3DDEB (ISNR = 8.06dB ), and our method (ISNR = 9.04dB).

number, all the ISNR curves increase monotonically and ultimately become flat and stable, exhibiting good stability of the proposed model. One also can observe that 6 iterations ( $iter = 6$ ) are typically sufficient.

## 5. Conclusion

We have presented a new deconvolution method that uses a combination of the rolling guidance filter in the spa-



Figure 6. Details of the image deconvolution experiment on image *Barbara* ( $512 \times 512$ ). From left to right and top to bottom: original image, noisy and blurred image (scenario 2), the deblurred image by ForWaRD (ISNR=1.87dB), SURE-LET (ISNR=2.24dB), BM3DDEB (ISNR = 3.94dB ), and our method (ISNR = 5.15dB).

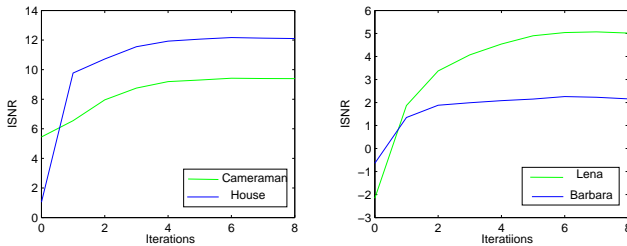


Figure 7. Change of the ISNR with iterations for the different setups of the proposed algorithm. Left: deblurring of *Cameraman* and *House* image, scenario 3; Right: deblurring of *Lena* and *Barbara* image, scenario 4.

tial domain and short-time Fourier transform (STFT) based shrinkage in the frequency domain. Rolling guidance filter has been proved to remove small-scale structures while preserving other content, parallel in terms of importance to previous edge-preserving filter, but it can not preserve low-contrast detail like textures. STFT shrinkage on the other hand results in good detail preservation, but it suffers from ringing artifacts near steep edges. We first integrate these two filters into the deconvolution problem to propose an efficient iterative algorithm, which leads to highquality results. Through twenty-four standard simulation experiments, it outperforms five existing state-of-the-art deconvolution algorithms.

## 6. Acknowledgements

We would like to thank the anonymous reviewers for their helpful feedback. This research is supported by

the National Science Foundation of China under Grant 61401425 and National Natural Science Foundation of China under Grant 61472157

## References

- [1] P. C. Hansen. *Rank-Deficient and Discrete Ill-Posed Problems: Numerical Aspects of Linear Inversion*. Philadelphia, PA: SIAM, 1998.
- [2] R. Neelamani, H. Choi, and R. G. Baraniuk. ForWaRD: Fourier-wavelet regularized deconvolution for ill-conditioned systems. *IEEE Trans. Signal Process.*, 52(2):418-433, 2004.
- [3] J. A. Guerrero-Colon, L. Mancera, and J. Portilla. Image restoration using space-variant Gaussian scale mixtures in overcomplete pyramids. *IEEE Trans. Image Process.*, 17(1):27-41, 2007.
- [4] A. Foi, K.Dabov, V.Katkovnik, and K.Egiazarian. Shape-adaptive DCT for denoising and image reconstruction. *In Soc. Photo-Optical Instrumentation Engineers*, volume 6064, pages 203-214, 2006.
- [5] K. Dabov, A.Foi, V.Katkovnik, and K.Egiazarian. Image restoration by sparse 3D transform-domain collaborative filtering. *In Soc. Photo-Optical Instrumentation Engineers*, volume 6812, page 6, 2008.
- [6] L. Rudin, S. Osher, and E. Fatemi. Nonlinear total variation based noise removal algorithms. *Physica D*, 60:259-268, 1992.
- [7] J. Portilla. Image restoration through 10 analysis-based sparse optimization in tight frames. *In IEEE Int. Conf Image Processing*, pages 3909-3912. IEEE, 2009.
- [8] F. Xue, F.Luisier, and T.Blu. Multi-Wiener SURE-LET Deconvolution. *IEEE Trans. Image Process.*, 22(5):1954-1968, 2013.
- [9] C.Jia and B.Evans. Patch based image deconvolution via joint modeling of sparse priors. *In IEEE Int. Conf Image Processing*, pages 681-684. IEEE, 2011.
- [10] L.Yuan, J.Sun, L. Quan, H.-Y.Shum. Image deblurring with blurred/noisy image pairs. *ACM Trans. on Graph.* volume 26, page 3. ACM, 2007.
- [11] L.Yuan, J.Sun, L. Quan, H.-Y.Shum. Progressive Inter-scale and Intra-scale Non-blind Image Deconvolution. *ACM Trans. on Graph.* volume 27, page 3. ACM, 2008.
- [12] Y. Wang, J. Yang, W. Yin, and Y. Zhang. A new alternating minimization algorithm for total variation image reconstruction. *SIAM J. Imag. Sci.*, 1(3):248-272, 2008.
- [13] J. Oliveira, J. M. Bioucas-Dias, and M. A. Figueiredo. Adaptive total variation image deblurring: A majorization-minimization approach. *Signal Processing*, 89(9):1683-1693, 2009.
- [14] O.V. Michailovich. An Iterative Shrinkage Approach to Total-Variation Image Restoration. *IEEE Trans. Image Process.*, 20(5):1281-1299, 2011.

- [15] W. Dong, L. Zhang, G. Shi, and X. Wu. Image deblurring and super-resolution by adaptive sparse domain selection and adaptive regularization. *IEEE Trans. Image Process.*, 20(7):1838-1857, 2011.
- [16] W. Dong, L. Zhang, G. Shi, and X. Li. Nonlocally centralized sparse representation for image restoration. *IEEE Trans. Image Process.*, 22(4):1620-1630, 2013.
- [17] J. Mairal, F. Bach, J. Ponce, G. Sapiro, and A. Zisserman. Non-local sparse models for image restoration. In *IEEE Int. Conf. Comput. Vision*, pages 2272-2279. IEEE, 2009.
- [18] W. Dong, G. Shi, and X. Li. Nonlocal image restoration with bilateral variance estimation: A low-rank approach. *IEEE Trans. Image Process.*, 22(2):700-711, 2013.
- [19] H. Ji, C. Liu, Z. Shen, and Y. Xu. Robust video denoising using low rank matrix completion. In *IEEE Int. Conf. Comput. Vision and Pattern Recognition*, pages 1791-1798. IEEE, 2010.
- [20] H. Ji, S. Huang, Z. Shen, and Y. Xu. Robust video restoration by joint sparse and low rank matrix approximation. *SIAM J. Imag. Sci.*, 4(4):1122-1142, 2011.
- [21] Q.Zhang, X.Y.Shen, L.Xu, and J.Y.Jia. Rolling guidance filter. In *Europ. Conf.Comput.Vision*. IEEE, 2014.
- [22] S.Paris, S. W.Hasinoff, and J.Kautz. Local Laplacian filters: Edge-aware image processing with a Laplacian pyramid. In *ACM Trans. Graphics*, volume 30, page 68. ACM, 2011.
- [23] C.Tomasi, and R.Manduchi. Bilateral filtering for gray and color images. In *IEEE Int. Conf. Comput. Vision*, pages 839-846. IEEE, 1998.
- [24] K. He, J. Sun, X. Tang. Guided image filtering. In *Europ. Conf.Comput.Vision*. IEEE, 2010.
- [25] J. F.Aujol, G. Gilboa, T.Chan, and S.Osher. Structure-texture image decomposition: modeling, algorithms, and parameter selection. *International Journal of Computer Vision*, 67(1):111-136, 2006.
- [26] A.Buades, T. M.Le, J.M.Morel, and L.A.Vese. Fast cartoon+texture image filters. *IEEE Trans. Image Processing.*, 19(8):1978-1986, 2010.
- [27] L.Xu, C.Lu, Y.Xu, and J.Jia. Image smoothing via L0 gradient minimization. In *ACM Trans. Graphics* volume 30, page 174. ACM, 2011.
- [28] G. Petschnigg. Digital photography with flash and no-flash image pairs. In *SIGGRAPH*:664-672, 2004.
- [29] K. Dabov, A. Foi, V. Katkovnik, and K. Egiazarian. Image denoising by sparse 3D transform-domain collaborative filtering. *IEEE Trans. Image Process.*, 16(8):2080-2095, 2007.
- [30] H.Yang, M.Zhu, X.T.Wu, Z.B.Zhang, and H.Y.Huang. Dictionary learning approach for image deconvolution with variance estimation. *Applied Optics*, 53(24):5677-5683, 2014.